IEEE Access
Multidisciplinary ⋮ Rapid Review ⋮ Open Access Journal

Received 4 June 2024, accepted 23 June 2024, date of publication 26 June 2024, date of current version 3 July 2024.

Digital Object Identifier 10.1109/ACCESS.2024.3419561

RESEARCH ARTICLE

Voltage Control of PEM Fuel Cell in a DC Microgrid Using Optimal Artificial Rabbits Algorithm-Based Fractional Order PID Controller

ANDREW J. RIAD[1], HANY M. HASANIEN[1,2], (Senior Member, IEEE), ZIA ULLAH[3], (Member, IEEE), ABDULAZIZ ALKUHAYLI[4], (Member, IEEE), AND AHMED H. YAKOUT[1]

[1]Electrical Power and Machines Department, Faculty of Engineering, Ain Shams University, Cairo 11517, Egypt
[2]Faculty of Engineering and Technology, Future University in Egypt, Cairo 11835, Egypt
[3]School of Electric Power, Civil Engineering and Architecture, Shanxi University, Taiyuan 030031, China
[4]Electrical Engineering Department, College of Engineering, King Saud University, Riyadh 11421, Saudi Arabia

Corresponding author: Hany M. Hasanien (hanyhasanien@ieee.org)

This work was supported by King Saud University, Riyadh, Saudi Arabia, under Grant RSP2024R258.

ABSTRACT This article utilizes a Fractional Order Proportional-Integral-Derivative (FOPID) controller for voltage regulation of a Proton Exchange Membrane fuel cell (PEMFC) in DC Microgrids. The PEMFC is considered a promising candidate for integration into DC Microgrids. However, maintaining a stable and efficient operation requires precise voltage control, especially under varying load conditions and inherent nonlinearities. The FOPID controller tuned by artificial rabbits optimization algorithm (FOPID-ARO) is recommended to address this challenge, which extends the conventional PID controller by introducing two additional parameters: the fractional orders of the derivative and integral actions. This enhancement allows for a more flexible control strategy that is capable of handling the complex dynamics of PEMFCs more effectively than traditional PID controllers. The suggested controller effectiveness is assessed under different operational scenarios, such as load and solar irradiance variations, and compared with a PID controller tuned by the ARO algorithm (PID-ARO) and an FOPID controller tuned by the jellyfish search algorithm and grey wolf optimizer. Moreover, actual data on solar irradiance are considered. The findings indicate that the FOPID-ARO controller performs better than the PID-ARO controller in terms of dynamic response and minimizes steady-state error more effectively.

INDEX TERMS DC microgrid, fuel cell, optimization methods, photovoltaic.

I. INTRODUCTION

Since fossil fuels are decreasing worldwide and they affect the environment [1], renewable energy resources began replacing them recently [2] as they are clean, abundant, and do not produce harmful emissions [3]. One promising clean energy source is fuel cells (FCs), as their energy is not intermittent since they do not depend on weather conditions, time, and location, unlike solar and wind energy [3], [4]. They continue to produce electricity provided that they are supplied with fuel, and they are more stable and rigid than other renewable energy resources as their inputs (hydrogen and oxygen) have low variability, unlike wind and solar energy. Moreover, they can be used as a backup power source in DC microgrids instead of conventional batteries due to their high operating hours, which is similar to telecommunication-related applications [5]. They also can enhance the power quality of the microgrid and strengthen local reliability by balancing power supply and demand, reducing power fluctuations caused by renewable energy resources, and integrating with the electrolyzer to store excess energy for later use in the form of hydrogen [6]. Additionally, they can

The associate editor coordinating the review of this manuscript and approving it for publication was Arturo Conde.

provide steady power, and when the load exceeds the PV capacity, they supply the energy needed [7] and, they are characterized by the flexibility of fuel [8].

FCs are classified according to the type of electrolyte they utilize, including PEMFC, alkaline FC, phosphoric acid FC, molten carbonate FC, and solid oxide FC. PEMFC produces water and electricity by undergoing a chemical reaction between the two gases of oxygen and hydrogen [9]. PEMFC has many advantages, such as being lightweight, having no waste material, being a fast startup, being highly efficient, and having a low operating temperature [2], [10]. However, it has some demerits, such as sensitivity to carbon monoxide, expensive metal catalysts, and complex thermal and water management [11]. Also, as the temperature increases or the relative humidity decreases, the proton conductivity of PEMFC decreases [12].

Since the PEMFCs V-I characteristics are nonlinear and depend on the cell temperature and the oxygen and hydrogen partial pressures, many controllers and algorithms have been adopted to maximize the FC's output power or control its output voltage [13]. So, researchers used many maximum power point tracking (MPPT) techniques to get the fuel cell's peak power. Ahmadi and others [13] utilized an MPPT method with a (PID) controller tuned by the particle swarm optimization algorithm (PSO). They demonstrated that compared to sliding mode and perturb and observe algorithms, the PSO-PID controller has very low power fluctuations and high accuracy. In [14], Derbeli and others utilized a second-order super-twisting algorithm with a sliding mode controller to maximize the output power. At the same time, Souissi [15] used a super-twisting algorithm with an adaptive sliding mode controller. Reference [16] used an MPPT based on the backstepping algorithm and a current reference estimator. An MPPT based on the eagle strategy and a fuzzy logic controller (FLC) were proposed in [17]. In contrast, an MPPT controller with a neural network incremental conductance-based variable step size was introduced by Harrag and Bahri [18]. They found that steady-state oscillations and convergence speed operate better than conventional variable and fixed step size MPPT. Gulzar [19] used a fractional order PID (FOPID) controller with an optimal salp swarm algorithm. Avanki and Sarvi [20] used a PID controller and an MPPT based on a water cycle algorithm (WCA) and compared its performance with the current-based MPPT method (CMPPT), voltage-based MPPT method (VMPPT), and perturb and observe method. Moreover, Liu and others [21] used an MPPT with a fractional order high pass filter based on extremum-seeking control. Fuzzy control with an artificial bee colony algorithm is utilized to obtain the PEMFC maximum power [22]. Reference [23] used the grey wolf optimizer (GWO) to optimize the PID controller parameters. Qi and others introduced a FOPID controller optimized by PSO in [24]. Ali and others [25] used a modified manta ray foraging algorithm to optimize an adaptive neuro-fuzzy inference system (ANFIS) for MPPT of PEMFC. Moreover, an MPPT controller based on a golden section search algorithm is presented in [26]. Fathy and others [27] used a forensic-based investigation algorithm to optimize a FOPID-based MPPT. In [28], the parameters of an FLC are optimized by an equilibrium optimizer to obtain the PEMFC maximum output power.

Maintaining the voltage constant at the load is also essential, so the researchers used different algorithms to optimize the controller parameters to enhance the output voltage by decreasing fluctuations and overshoots in transient states. Benchouia and others [29] introduced an adaptive fuzzy controller to keep a constant output voltage by controlling the input gasses flow rate. According to their findings, the adaptive fuzzy controller outperformed the PI controller in terms of settling times and rise time. Cao and others [30] controlled the PEMFC output voltage by designing a linear quadratic regulator (LQR) optimized by an improved chaotic whale optimization algorithm. Moreover, Salah and others [31] used a PI controller tuned by the African vulture optimization algorithm (AVOA) to control the output voltage. It showed an improvement in settling time, maximum percentage undershoot, and maximum percentage overshoot compared to a PI controller tuned by PSO. In [32], a dynamic integral sliding mode control is proposed, and its performance is compared to a PI controller. Furthermore, Hamedi and others [33] used a bacterial foraging algorithm (BFA) to tune a lead-lag controller. Dhahad and others [34] used different optimization algorithms, such as a chaotic particle swarm, firefly, and hybrid firefly-chaotic particle swarm with a single-input multi-output PID neural network controller. Kart and others [35] utilized a fuzzy logic controller to keep a constant output voltage, yielding a better fuel cell dynamic performance than the PID controller. Moreover, Li and others [36] used an ambient intelligence exploration multi-delay deep deterministic policy gradient (AIEM-DDPG) algorithm with an adaptive PI controller to control the voltage. In contrast, Wang and others [37] controlled the output voltage by proposing an improved fuzzy PID control method. In [38], a model predictive control algorithm based on a neural network was proposed for voltage control. The authors in [39] controlled the PEMFC voltage using an ANFIS-based model predictive controller (MPC). It had smaller overshoots and a lower settling time than the adaptive PID controller. Li and others [40] designed a PID controller and an MPC controller to control the fuel and airflow rates of PEMFC and maintain a constant output voltage. According to their findings, the MPC controller outperformed the PID controller as it had a more minor overshoot and faster response.

Although the above controllers are characterized by flexibility, stability, and robustness, such as sliding model control, predictive model control, etc., they have some drawbacks. Sliding mode control is not easy to use. Its design is complex and suffers from long computational time [41]

and chattering phenomenon [42]. From the characteristics of MPC controllers is their capacity to apply the input-output constraints during the optimization process, but they have complex computations [43] and have large overshoots [44]. FLC suffers from difficulties in implementation due to its expensive processing power requirements [45], its response contains oscillations [46], and it needs more memory, which makes it more expensive [47]. Using the PID controller with a nonlinear system can harm the converter because of the converter's dynamic response to overshoots [35]. Also, it has a slow response [13]. External disturbances can adversely affect The PI controller's performance despite its unique simplicity [48]. Furthermore, the PI, PD, and PID controllers are very sensitive to significant load variations. Both ANFIS and neural network algorithms have a lot of parameters that need to be adjusted. Moreover, ANFIS has a high computational cost and needs large data for learning and training [19], [49]. For the reasons mentioned above, the FOPID controller is suggested for regulating the PEMFC output voltages as it has many merits, including high disturbance rejection, its enhanced processing ability to tolerate the uncertainties of models in real-time and nonlinear applications, and its improved set-point tracking [50]. Also, it is less susceptible to variations in the controlled system parameters [51] and is more robust and flexible than an integer order PID controller [52]. Moreover, it improves the dynamic stability against small signal variations [53].

To integrate multiple examples of renewable resources for energy, such as solar photovoltaic (PV) and FC, with energy storage (ES) systems, such as supercapacitors and batteries, to provide power to DC loads, DC microgrids are becoming a more viable option [31]. Microgrids have three types: DC, AC, and hybrid AC/DC microgrids [54], with two operating modes: islanded mode (off-grid) and grid-connected mode [55]. DC microgrids have a few merits over AC ones, such as lower power losses and no need for reactive power and frequency control, so they are simpler to control than AC ones [56]. However, one of the main challenges of DC microgrids is the voltage and power control as most renewable energy sources suffer from the intermittency problem, as mentioned before, plus the load uncertainties causing fluctuation in the voltage so the fuel cell is used as a backup power which depends on the fuel supplied to it [31], [57], [58]. One of the main methods for regulating the voltage of the islanded DC microgrids has been the droop control method, but it has some drawbacks like slow transient response, and it can lead to instability when subjected to nonlinear loads and load changes [59]. Droop control that is based on virtual resistance suffers from DC bus voltage deviation as load increases and unequal load distribution when converter line resistances differ [60].

In this paper, the voltage of a DC microgrid that consists of PV, PEMFC, and DC load is controlled by controlling the PEMFC DC-DC converter. A FOPID controller tuned by ARO is proposed for controlling the converter, and its performance is compared to that of a PID controller tuned by ARO under different variations of load and irradiance of PV. Also, the ARO algorithm is compared to the jellyfish search algorithm (JSA) and the GWO. The ARO algorithm is a novel technique first introduced by Wang and others [61]. It is based on two strategies that rabbits use for survival: detour foraging and random hiding [61]. In addition, it features a slight standard deviation and a fast convergence curve [9].

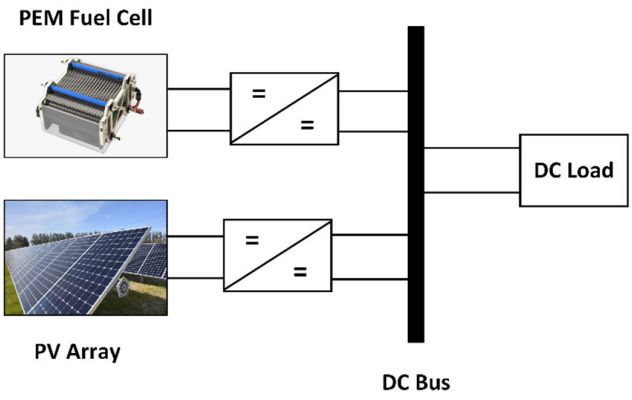

FIGURE 1. DC microgrid.

The following are this article primary contributions:

- The FOPID tuned by the ARO algorithm (FOPID-ARO) controls the fuel cell DC-DC converter to keep the microgrid voltage constant.
- The proposed control scheme is used to enhance the dynamic operation of DC microgrids.
- The performance of FOPID-ARO is compared to FOPID tuned by JSA and GWO and PID tuned by ARO under different loading conditions and variable irradiance of PV.

The subsequent sections of the article are arranged as follows: the design and modeling of the DC microgrid are shown in Section II. Section III shows the problem formulation, while Section IV demonstrates the ARO algorithm. Simulations, results, and comparisons are discussed in Section V, and the conclusions are summarized in Section VI.

II. MICROGRID MODELING

The DC microgrid considered in our study comprises a PV, a PEMFC, and a DC load, as shown in Fig. 1. A boost converter is connected to the PV panel. The converter control is based on incremental conductance MPPT presented in [62] and [63], and the boost converter design is described in [64]. Additionally, a boost converter is connected to the PEMFC. A FOPID controller tuned by the ARO algorithm is proposed to control this converter in order to keep the load voltage constant. A comparison is made between the PID and FOPID controller using the ARO algorithm, and the ARO is compared against the JSA and the GWO algorithms in different cases, which proves the superiority of the FOPID tuned by the ARO algorithm.

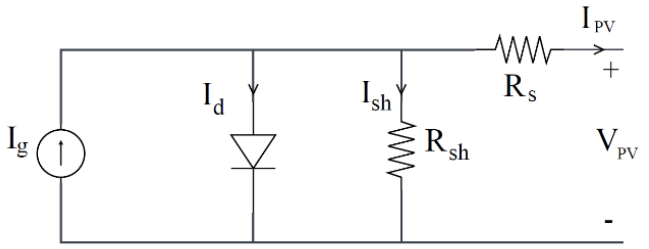

FIGURE 2. Model of PV cell.

A. PV MODEL

The PV cell can be represented by numerous models, including single, double, and triple diode models. Yet, the single-diode model is the most commonly utilized owing to its simplicity and precision [31], [63], [65]. The PV cell equivalent circuit constitutes a controlled current source. A diode is connected in a parallel position to the source. To keep the circuit realistic, shunt and series resistances are connected to represent power losses, as shown in Fig. 2 [63]. The nonlinear I-V characteristics of a PV array, which is constructed by PV modules connected in parallel and series combinations, are represented by the following equations [66]:

$$I_{PV} = \left(I_g - I_d - I_{sh}\right) \tag{1}$$

$$I_d = I_0\left[\exp\left(\frac{V_{PV} + I_{PV}R_s}{nV_t}\right) - 1\right] \tag{2}$$

$$I_{sh} = \frac{V_{PV} + I_{PV}R_s}{R_{sh}} \tag{3}$$

$$V_t = \frac{N_s kT}{q} \tag{4}$$

where I_{PV} and V_{PV} are the PV module output current and voltage, while V_t is the module's thermal voltage. I_g, I_d, I_0, and I_{sh} are the generated current by the PV due to sunlight, the current passing through the diode, the diode saturation current, and the leakage current in the PV cell's shunt resistor, which is denoted by R_{sh}, respectively. R_s represents the PV cell series resistance. The total number of cells connected in series within a module is denoted by N_s. n stands for the ideality factor, k is Boltzmann's constant (J/K), T is the PV cell's operating temperature (Kelvin), and q is the electronic charge (C). SunPower SPR-305-WHT is the type of PV module utilized in the simulation with a rating of 1.22 kW and Table 1 lists its parameters.

Since the load, temperature, and irradiance (weather conditions) affect the PV harvested power, potential level, and current, the PV array has a boost converter connected to it and is controlled by an MPPT technique to capture most of the resulting power. The MPPT method used is incremental conductance (IC), as it is characterized by its fast response to temperature and irradiance changes [63]. This method is described by Equations (5)-(8) [67]:

$$P = VI \tag{5}$$

TABLE 1. The PV array parameters.

Parameters	Value
No. of parallel strings	4
No. of cells per module	96
No. of modules per string	1
Voltage of module at maximum power V_m	54.7 V
Current of module at maximum power I_m	5.58 A
Maximum power of module P_m	305.226 W
Open circuit voltage of module V_{OC}	64.2 V
Short circuit current of module I_{SC}	5.96 A
Switching Frequency	5000 Hz
Boost converter capacitance	12000 µF
Boost converter inductance	5 mH

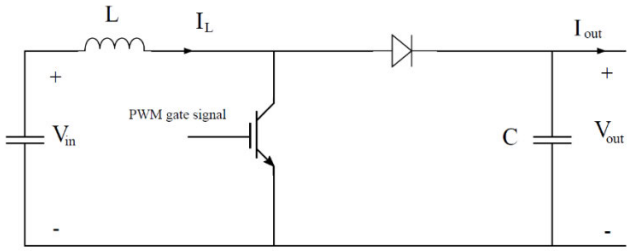

FIGURE 3. Boost converter.

$$\frac{\partial P}{\partial V} = I + V\frac{\partial I}{\partial V} \tag{6}$$

$$\text{at maximum power } \frac{\partial P}{\partial V} = 0 \tag{7}$$

$$\text{so, } \frac{\partial I}{\partial V} = -\frac{I}{V} \tag{8}$$

From the previous equations, this method focuses on varying the duty cycle to fulfill the condition $\left(\frac{\partial I}{\partial V} = -\frac{I}{V}\right)$.

B. DC-DC CONVERTER

The voltage of both the PV and the PEMFC is increased to the DC bus voltage (100V) through a boost converter seen in Fig. 3, whose dynamic equations are as follows [68]:

$$LxI_L = V_{in} - (1 - D)\,xV_{out} \tag{9}$$

$$CxV_{out} = (1 - D)\,xI_L - I_{out} \tag{10}$$

where inductance current and output current are denoted by I_L and I_{out}, while output voltage and input voltage are denoted by V_{out} and V_{in} respectively. D represents the duty ratio coming from the controller in the range of [0, 1]. The converter's inductance and capacitance are denoted by L and C and can be designed according to Equations (11) and (12) [64]:

$$L = \frac{V_{in}x(V_{out} - V_{in})}{F_s x\Delta I x V_{out}} \tag{11}$$

$$C = \frac{IoutxD}{F_s x\Delta V} \tag{12}$$

where ΔV, ΔI, and F_s are voltage ripples, current ripples, and switching frequency, respectively. The current ripples, the voltage ripples, and the output voltage are determined using the following equations [69]:

$$V_{out} = \frac{V_{in}}{1 - D} \tag{13}$$

$$\Delta V = \frac{I_{out} x D}{F_s x C} \tag{14}$$

$$\Delta I = \frac{V_{in} x D}{F_s x L} \tag{15}$$

C. FUEL CELL DYNAMIC MODEL

The PEMFC produces electricity with water as a side product through the chemical reaction between the two gases of oxygen and hydrogen. Equations (16) and (17) describe the reaction occurring for the two gases at the cathode and the anode, respectively [70]. The FC can be represented as a controlled voltage source that has activation losses and ohmic losses, as stated in [22] and [71]. The PEMFC stack output voltage (V_{Stack}) is calculated using Equations (18) to (26) as in [22]. For more details about the PEMFC model, check [72].

$$\text{Cathode} : O_2 + 4e^- + 4H^+ \rightarrow 2H_2O + \text{energy} \tag{16}$$

$$\text{Anode} : 2H_2 + 4H^+ \rightarrow 4e^- \tag{17}$$

$$V_{Stack} = N_c K_c E_{Nernst} - N_c V_{ohm} - N_c V_{act} \tag{18}$$

where K_c denotes the voltage constant under standard operating conditions, and N_c is the number of cells. E_{Nernst} and V_{Stack} represent the Nernst voltage and the stack's output voltage, respectively, while the ohmic voltage drop and the activation voltage drop are denoted by V_{ohm} and V_{act}. These voltages can be calculated by:

$$E_{Nernst} = \frac{RT}{zF} \ln\left(P_{H2}\sqrt{P_{O2}}\right) + (T - 298)\frac{-44..43}{zF} + 1.229 \tag{19}$$

$$V_{act} = \frac{RT}{z\alpha F} \ln\left(\frac{I_{FC}}{I_0}\right) \frac{1}{(sT_d/3) + 1} \tag{20}$$

$$V_{ohm} = I_{FC} R_{ohm} \tag{21}$$

where the universal gas constant (J/mol K) is denoted by R, while F represents Faraday's constant (A s/mol), FC's operating temperature (Kelvin) is denoted by T, and z is the number of moving electrons (z=2). α denotes the transfer coefficient of the charge, I_{FC} is the PEMFC stack output current (A), I_0 is exchange current (A), R_{ohm} denotes the internal resistance of PEMFC (electrodes and electrolyte resistance), T_d denotes the stack settling time, hydrogen, and oxygen partial pressures (atm) are denoted by P_{H2} and P_{O2} respectively. P_{H2},P_{O2}, and I_0 are represented as follows:

$$P_{H2} = (1 - \lambda_{H2}) \times x \times P_{fuel} \tag{22}$$

$$P_{O2} = (1 - \lambda_{O2}) \times y \times P_{air} \tag{23}$$

$$I_0 = \frac{zFk\,(P_{H2} + P_{O2})}{Rh} \exp\left(\frac{-\Delta G}{RT}\right) \tag{24}$$

TABLE 2. PEMFC parameters.

Parameters	Value
N_c	65
T	65^0C
x	99.95%
y	21%
P_{air}	1 bar
P_{fuel}	1.5 bar
$V_{nominal}$	45 V
$I_{nominal}$	133.3 A
Boost converter inductance	0.5 mH
Boost converter capacitance	7500 µF

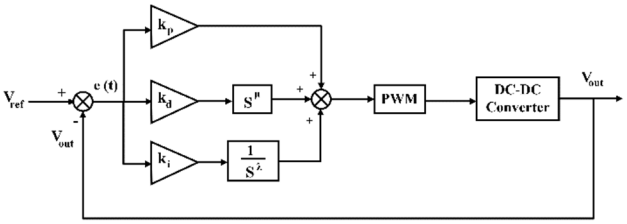

FIGURE 4. FOPID controller block diagram.

where x and y denote the fuel's hydrogen percentage and the air's oxygen percentage, respectively, while P_{air} and P_{fuel} stand for the air and fuel supply pressures (atm), respectively. ΔG is the activation energy barrier (J), k stands for Boltzmann's constant (J/K), while h represents Planck's constant (Js). λ_{O2} and λ_{H2} denote the conversion rates of oxygen and hydrogen that can be described as follows:

$$\lambda_{H2} = \frac{60000 RT I_{FC}}{zFP_{fuel}Q_{fuel}x} \tag{25}$$

$$\lambda_{O2} = \frac{60000 RT I_{FC}}{2zFP_{air}Q_{air}y} \tag{26}$$

where Q_{air} and Q_{fuel} represent the air and fuel flow rates (L/min), respectively. Finally, the PEMFC stack output power (P_{Stack}) is calculated as follows:

$$P_{Stack} = V_{Stack} I_{FC} \tag{27}$$

The FC's output voltage is augmented to the DC-bus voltage of 100 V. A PEMFC module of 6 kW, according to the above model, is utilized in our simulation. Table 2 provides the main parameters of the FC [72].

D. THE PROPOSED FOPID CONTROLLER

The FOPID controller is utilized to maintain a constant voltage at the load and to enhance its dynamic response. In comparison to PID controllers, FOPID controllers have two more parameters (λ and μ), which make them more flexible and robust [73]. The FOPID controller block diagram is depicted in Fig. 4, and equations (28) and (29) provide the output equations in the time and frequency domains,

TABLE 3. Parameters boundaries for PID controller.

	k_p	k_i	k_d
Min Value	0	0.6	0
Max Value	0.1	0.7	0.01

respectively.

$$f(t) = e(t)\left(k_d D^{\mu} + k_i D^{-\lambda} + k_p\right) \quad (28)$$

$$F(s) = k_d s^{\mu} + k_i s^{-\lambda} + k_p \quad (29)$$

where k_i is the constant of integration, k_p is the proportional constant, and k_d is the differentiation constant. The fractional orders of the differentiating and integrating actions are denoted by μ and λ, respectively.

III. PROBLEM FORMULATION

As mentioned before, by controlling the PEMFC's DC-DC converter through either a PID controller or a FOPID controller, the DC microgrid's voltage is kept constant. The FOPID controller has five parameters (k_p, k_i, k_d, λ, and μ) to be optimized, while the PID controller only has three (k_p, k_i, and k_d). To determine these parameters' optimum values, the ARO algorithm is utilized to minimize the objective function (OF). The targeted OF is the integral square error (ISE) of the voltage difference between the microgrid's output voltage (or load voltage) and the reference voltage as shown in equation (30) while keeping the controller parameters within a predefined range shown in Tables 3 & 4.

$$ISE = \int_0^{t_s} (V_{load} - V_{ref})^2 dt \quad (30)$$

where t_s is the simulation time.

IV. OPTIMIZATION ALGORITHMS

A. GREY WOLF OPTIMIZER (GWO)

The GWO algorithm is based on the hierarchy of grey wolves and how they hunt. They have four main types: alpha, beta, delta, and omega. The alpha is the pack leader. Beta keeps an eye on the pack's other members and ensures that they follow orders. The omegas, the lowest rank in the group, are dominated by delta wolves, who follow the orders of alpha and beta. Delta wolves perform various tasks, including watching their territory, tending to sick members, and helping in attacking their prey. Grey wolves follow three steps in hunting their prey: searching for the prey, surrounding the prey, and finally, attacking the prey. The following equations are used to update the grey wolves' positions and are summarized in Fig. 5. For more information, check [74].

$$\vec{D} = \left|\vec{X_p}(t) \cdot \vec{C} - \vec{X}(t)\right| \quad (31)$$

$$\vec{X}(t+1) = \vec{X_p}(t) - \vec{D} \cdot \vec{A} \quad (32)$$

$$\vec{A} = 2 \times \vec{r_1} \cdot \vec{a} - \vec{a} \quad (33)$$

$$\vec{C} = 2 \times \vec{r_2} \quad (34)$$

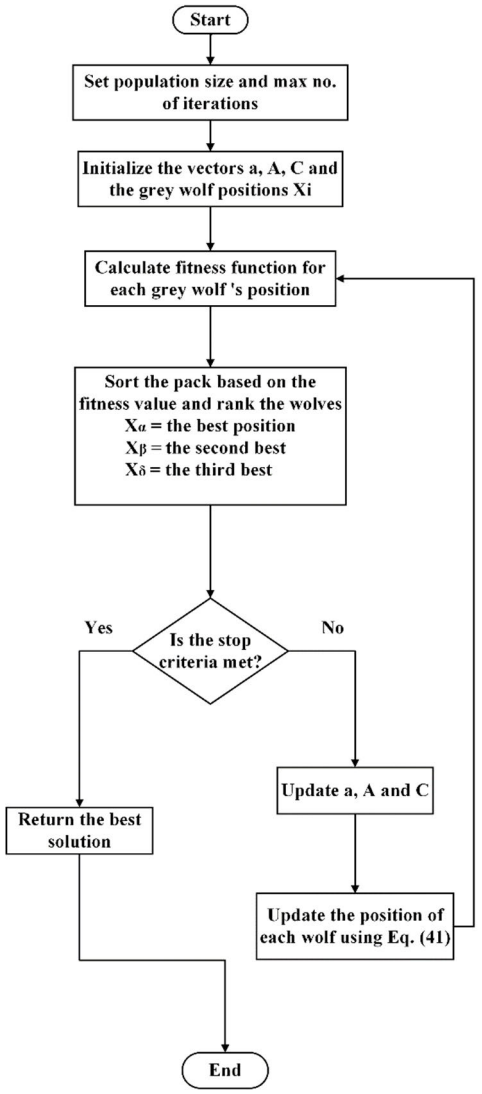

FIGURE 5. Grey wolf optimizer algorithm.

where $\vec{X_p}(t)$ is the prey's position vector, while $\vec{X}(t)$ is the grey wolf's position vector. t is the iteration number and coefficient vectors are denoted by $\vec{C}$ and $\vec{A}$. $\vec{r_1}$ and $\vec{r_2}$ are random vectors between (0,1), while $\vec{a}$ is a vector that decreases linearly from 2 to 0 during the iterations. Equation (32) represents the three steps of hunting. It shows that when $\left|\vec{A}\right| > 1$ the wolves search for the prey (exploration), when $\left|\vec{A}\right| = 1$ they surround the prey and when $\left|\vec{A}\right| < 1$ they attack the prey (exploitation).

The behavior of grey wolves while hunting can be mathematically described by taking into account the position of alpha, beta, and delta, which possess better information regarding the location of the prey. So, alpha is the best solution, while beta and delta are the second-best and third-best solutions, respectively. Wolves update their positions according to these three best positions using Equation (41).

$$\vec{D_\alpha} = \left|\vec{X_\alpha} \cdot \vec{C_1} - \vec{X}\right| \quad (35)$$

$$\overrightarrow{D_\beta} = \left|\overrightarrow{X_\beta}.\overrightarrow{C_2} - \overrightarrow{X}\right| \quad (36)$$

$$\overrightarrow{D_\delta} = \left|\overrightarrow{X_\delta}.\overrightarrow{C_3} - \overrightarrow{X}\right| \quad (37)$$

$$\overrightarrow{X_1} = \overrightarrow{X_\alpha} - \overrightarrow{D_\alpha}.\overrightarrow{A_1} \quad (38)$$

$$\overrightarrow{X_2} = \overrightarrow{X_\beta} - \overrightarrow{D_\beta}.\overrightarrow{A_2} \quad (39)$$

$$\overrightarrow{X_3} = \overrightarrow{X_\delta} - \overrightarrow{D_\delta}.\overrightarrow{A_3} \quad (40)$$

$$\overrightarrow{X}\,(t+1) = \frac{\overrightarrow{X_1} + \overrightarrow{X_2} + \overrightarrow{X_3}}{3} \quad (41)$$

B. JELLYFISH SEARCH ALGORITHM (JSA)

The way jellyfish move and search for food in the ocean served as inspiration for the JSA algorithm. Their movement is based on three rules: (a) they either move based on the direction of the ocean current or move inside a group (swarm), (b) they are attracted to areas with higher food concentrations, (c) The location and its associated objective function determine the amount of food found. A time control mechanism will determine if they will move inside a group or follow the ocean current [75]. The following sections include the equations used to update the positions of the jellyfish, which are summarized in Fig. 6. Refer to [75] for additional information.

1) OCEAN CURRENT

Jellyfish are attracted to the food contained in the ocean current. By averaging all of the vectors from every jellyfish in the ocean to the jellyfish that is now in the best position, the direction of the ocean current is ascertained, as shown in Equation (42), and the updated location of each jellyfish is given by Equation (43).

$$\overrightarrow{OD} = X^* - \mu \times \text{rand} \times \beta \quad (42)$$

$$X_i\,(t+1) = \text{rand} \times \overrightarrow{OD} + X_i\,(t) \quad (43)$$

where $\overrightarrow{OD}$ is the direction of ocean current, while X_i and X^* represent the position of each jellyfish and the position of the jellyfish with the best fitness, respectively. The mean position of all jellyfish is denoted by μ, while β is a distribution coefficient.

2) JELLYFISH SWARM

When jellyfish move in a swarm, they have two types of motion: passive and active. In passive motion, jellyfish move around their locations, and their updated positions are given by Equation (44).

$$X_i\,(t+1) = (B_u - B_l) \times \text{rand} \times \gamma + X_i\,(t) \quad (44)$$

where γ is a coefficient based on the length of motion of the jellyfish, while the lower and upper bounds of search space are denoted by B_l and B_u respectively. In active motion, the jellyfish move toward the position with large amounts of food. The direction of motion is determined by comparing the amount of food at the position of the jellyfish of interest and a jellyfish selected at random, as shown in Equation (45), and the updated location of each jellyfish is given by Equation (46).

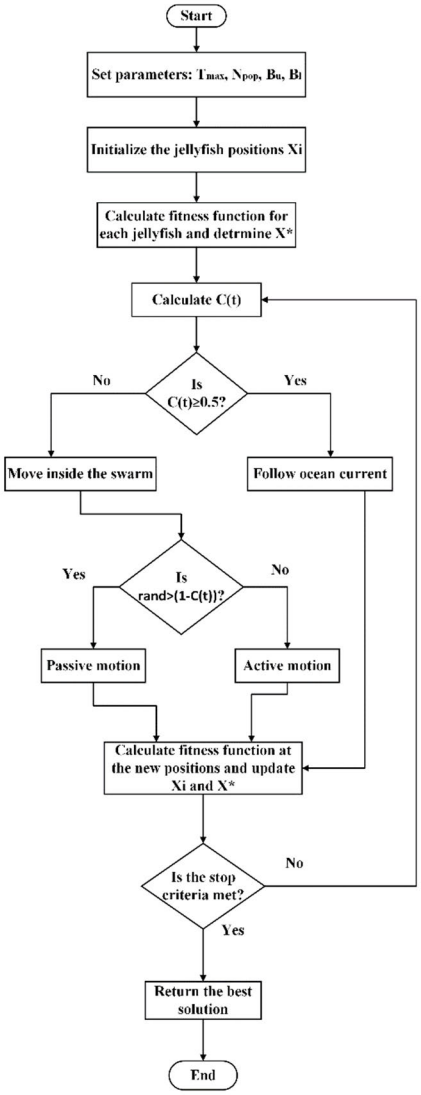

FIGURE 6. Jellyfish search algorithm.

$$\overrightarrow{Dir} = \begin{cases} X_j\,(t) - X_i\,(t)\,, & f\left(X_j\right) \le f\,(X_i) \\ X_i\,(t) - X_j\,(t)\,, & otherwise \end{cases} \quad (45)$$

$$X_i\,(t+1) = rand \times \overrightarrow{Dir} + X_i\,(t) \quad (46)$$

where $\overrightarrow{Dir}$ is the direction of motion of the jellyfish and X_j is the position of a randomly selected jellyfish.

3) TIME CONTROL MECHANISM

As mentioned before, the jellyfish either follow the ocean current or move in a swarm with two types of motion: active and passive. So, a time control function C(t) (ranges between 0 and 1) is used to determine which type of motion the jellyfish will do. When C(t) is greater than or equal to 0.5, they follow the ocean current; otherwise, they move inside a swarm. The value of (1-C(t)) is compared with a random

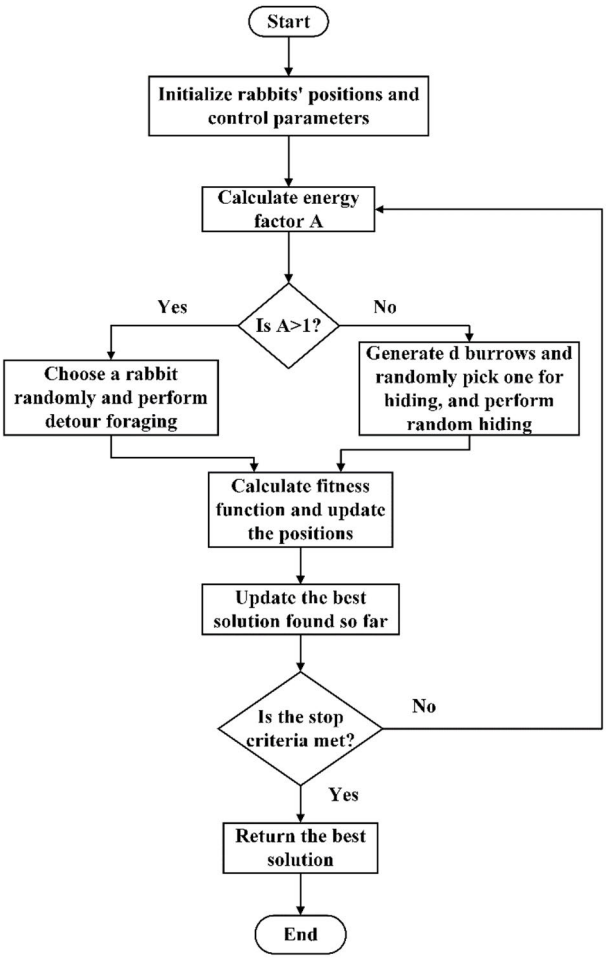

FIGURE 7. Artificial rabbits optimization algorithm flowchart.

number to decide which type of motion the jellyfish will do when moving in a swarm (active or passive).

$$C(t) = \left|(2 \times \text{rand} - 1) \times \left(1 - \frac{t}{T_{max}}\right)\right| \tag{47}$$

where t is the iteration number, and T_{max} is the maximum number of iterations.

C. ARTIFICIAL RABBITS OPTIMIZER (ARO)

The ARO algorithm draws its inspiration from the survival strategies used by rabbits. They use a strategy referred to as ''detour foraging'' to look for food at a distance from their nests. Around their nests, they dig burrows and choose one at random to hide in to evade hunters and predators; this tactic is known as random hiding. They will decide between detour foraging and random hiding according to their energy. When their energy is high enough, they will search far from their nests for food, a process known as detour foraging. When their energy levels are low, they will hide randomly in one of the burrows around them. The equations utilized for updating the rabbits' positions are given in the following sections, and Fig. 7 summarizes them. Refer to [61] for more information.

1) ENERGY SHRINKAGE (EXPLORATION AND EXPLOITATION SWITCHING)

The amount of energy a rabbit possesses determines whether it will detour foraging or hide randomly. Hence, equation (48) is used to calculate an energy factor A(t). A rabbit will resort to random hiding when A(t) is less than or equal to 1 and will undertake detour foraging when A(t) is greater than 1.

$$A(t) = 4\left(1 - \frac{t}{T_{max}}\right)\ln\frac{1}{a_1} \tag{48}$$

where a_1 is a random number between (0,1) and T_{max} represents a maximum number of iterations.

2) DETOUR FORAGING (EXPLORATION)

In order to distance predators from their nests, rabbits seek food in locations far from their homes. Equation (49) indicates that the rabbits' search for food is random and influenced by the rabbits' relative positions to each other.

$$\vec{y}_i(t+1) = round\,(0.5 \times (0.05 + a_2)) \times n_1 + \vec{u}_j(t) + K \times \left(\vec{u}_i(t) - \vec{u}_j(t)\right), i, j = 1, .., n \text{ and } j \neq i \tag{49}$$

$$K = L \times f \tag{50}$$

$$L = (e - e^{\left(\frac{t-1}{T_{max}}\right)^2}) \times sin(2\pi a_3) \tag{51}$$

$$f(v) = \begin{cases} 1 & if\ v == x(z) \\ 0 & else \end{cases} \quad v = 1, \ldots, d \text{ and } z = 1, \ldots, [a_4.d] \tag{52}$$

$$x = rand\ perm(d) \tag{53}$$

$$n_1 \sim N(0, 1) \tag{54}$$

where $\vec{u}_i(t)$ and $\vec{y}_i(t+1)$ represents the *i*th rabbit's location and the candidate's location of the *i*th rabbit at the time *t* and *t+1,* respectively. f is a mapping vector, d represents the number of variables to be optimized in the problem (3 or 5 in our case), and n represents the size of the rabbit population. a_2, a_3, and a_4 are three numbers chosen at random between (0,1) and n_1, which are subject to the standard normal distribution. L describes the rabbits' movement pace, while the rabbits' running characteristics are simulated by a running operator, which is denoted by K.

3) RANDOM HIDING (EXPLOITATION)

To evade predators and hunters, rabbits randomly select one of their burrows to hide in. A single rabbit possesses d burrows near the nest. The generation of these burrows for each rabbit is described by Equation (55).

$$\vec{b}_{i,j}(t) = \vec{u}_i(t) \times (H \times x + 1), i = 1, \ldots, n \text{ and } j = 1, \ldots, d \tag{55}$$

$$H = \frac{T_{max} - t + 1}{T_{max}} \times a_5 \tag{56}$$

$$x(v) = \begin{cases} 1 & if\ v == j \\ 0 & else \end{cases} \quad v = 1, \ldots\ldots, d \tag{57}$$

TABLE 4. Parameters boundaries for FOPID controller.

	k_p	k_i	k_d	λ	μ
Min Value	0	0.6	0	0	0
Max Value	0.1	0.7	0.01	1	1

TABLE 5. Parameters of PID and FOPID controllers.

Parameters	PID ARO	FOPID GWO	FOPID JSA	FOPID ARO
k_p	0.00042069	0.00130029	0.01199074	0.02468789
k_i	0.60773645	0.6	0.63297547	0.63928476
k_d	0.00061456	0.00067149	0.00065168	0.00056622
λ	-	0.79723420	0.90691209	0.98027444
μ	-	0.95046490	0.95013117	0.99241631

$$\overrightarrow{y}_i(t+1) = K \times \left(a_5 \times \overrightarrow{b}_{i,r}(t) - \overrightarrow{u}_i(t)\right) + \overrightarrow{u}_i(t), \quad i = 1, \ldots, n \tag{58}$$

$$x_r(v) = \begin{cases} 1 & if\ v == [a_6.d] \\ 0 & else \end{cases} \quad v = 1, \ldots\ldots, d \tag{59}$$

$$\overrightarrow{b}_{i,r}(t) = \overrightarrow{u}_i(t) \times (H \times x_r + 1), i = 1, \ldots\ldots, n \tag{60}$$

$$\overrightarrow{u}_i(t+1) = \begin{cases} \overrightarrow{y}_i(t+1), f(\overrightarrow{u}_i(t)) > f(\overrightarrow{y}_i(t+1)) \\ \overrightarrow{u}_i(t), f(\overrightarrow{u}_i(t)) \leq f(\overrightarrow{y}_i(t+1)) \end{cases} \tag{61}$$

where a_5 and a_6 are random numbers between (0,1), $\overrightarrow{b}_{i,j}$ represents the jth burrow of the ith rabbit, while $\overrightarrow{b}_{i,r}$ is the burrow randomly picked for hiding by the ith rabbit, as outlined in Equation (60). and H represents the hiding parameter. Equation (58) indicates that the ith rabbit will modify its location based on the burrow chosen at random. Ultimately, following either random hiding or detour foraging, a rabbit shall abandon its current location followed by settling in the location of the candidate if the new location's fitness is considered better when compared to the present's, as explained in Equation (61).

V. SIMULATION RESULTS

The FOPID controller tuned by the ARO algorithm (FOPID-ARO) is evaluated by comparing it to the PID controller tuned by the ARO algorithm (PID-ARO) and to the FOPID controller tuned by jellyfish search algorithm (FOPID-JSA) and grey wolf optimizer (FOPID-GWO) through different cases of changing the irradiance of the PV and the load in steps. The ISE, maximum percentage undershoot (MPUS), and maximum percentage overshoot (MPOS) are used to evaluate the two controllers. Table 5 presents the parameters obtained by both controllers.

A. CASE (1): LOAD CHANGES

The system is subjected to sudden load changes while maintaining the temperature and irradiance values of PV at 25^0C and 1000 W/m^{2,} respectively. The load is reduced from 3000 to 2000 W at time = 1 s, then increased from 2000 to 3500 W at time = 2 s, and at time = 3 s, it changed from 3500 to 4000 W as shown in Fig. 8a. The impact on the load voltage due to sudden load changes is illustrated in Fig. 8b. It is shown in Table 6 that FOPID-ARO has the best performance, the least ISE, and the least rise time. It is also noted that the FOPID-ARO decreased the MPOS by 30.41%, 23.28%, and 14.85% when compared to PID-ARO, FOPID-GWO, and FOPID-JSA respectively, and the MPUS by 30.16%, 10.60%, and 9.46% when compared to PID-ARO, FOPID-GWO, and FOPID-JSA respectively. This means that the FOPID-ARO enhanced the dynamic response and acted faster than the PID controller in regulating the voltage; however, it should be mentioned that the FOPID caused small oscillations in the output voltage due to the derivative component and that it takes a longer time in its optimization process than the conventional PID controller as the FOPID has five parameters to be optimized while the PID has only three.

TABLE 6. The transient parameters and ISE of load voltage for case 1.

Parameters	PID ARO	FOPID GWO	FOPID JSA	FOPID ARO
ISE	0.454736093	0.231656371	0.223932042	0.204204119
MPUS (%)	2.078656482	1.623970118	1.603573901	1.451809971
MPOS (%)	1.460336368	1.324536250	1.193429879	1.016220452
Rise time (s)	0.02193	0.021255	0.0218	0.02097

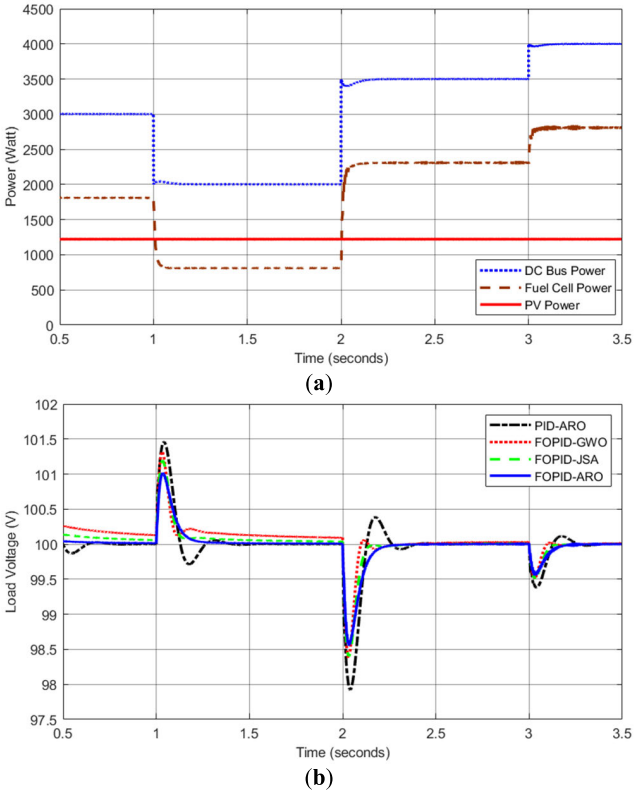

FIGURE 8. Case 1: (a) Load, FC, and PV power; (b) Load voltage.

B. CASE (2): IRRADIANCE CHANGES

Here, the system is tested against sudden changes in the irradiance of the PV while keeping the temperature of PV and the load constant at 25^0C and 3000 W, respectively. As shown

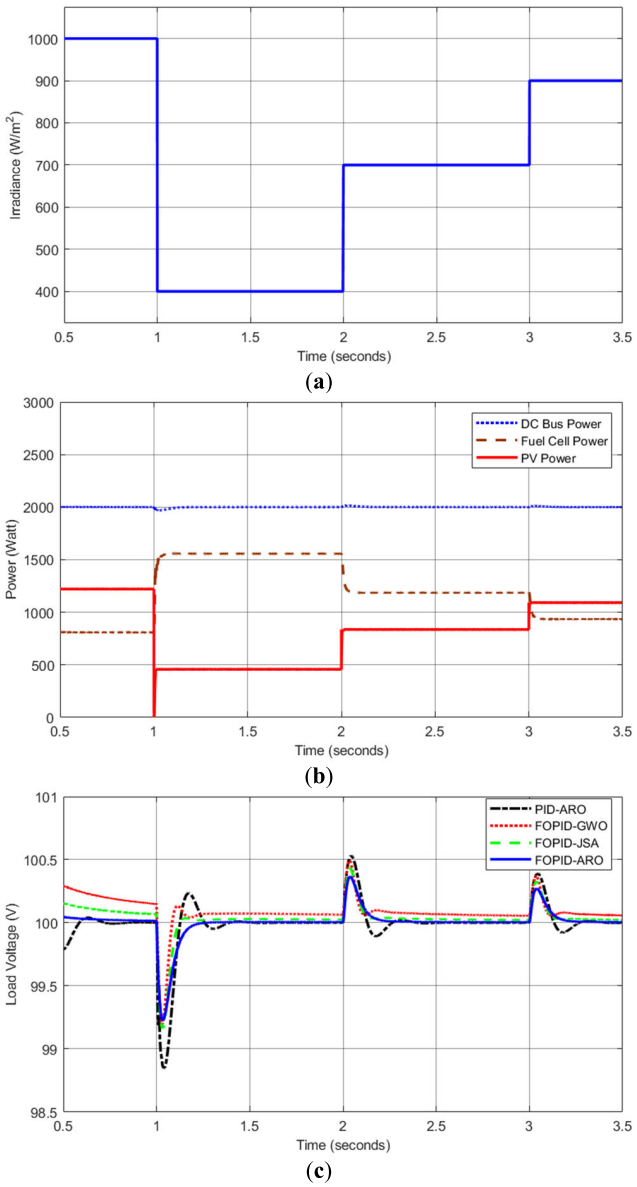

FIGURE 9. Case 2: (a) PV Irradiance; (b) Load, FC, and PV power; (c) Load voltage.

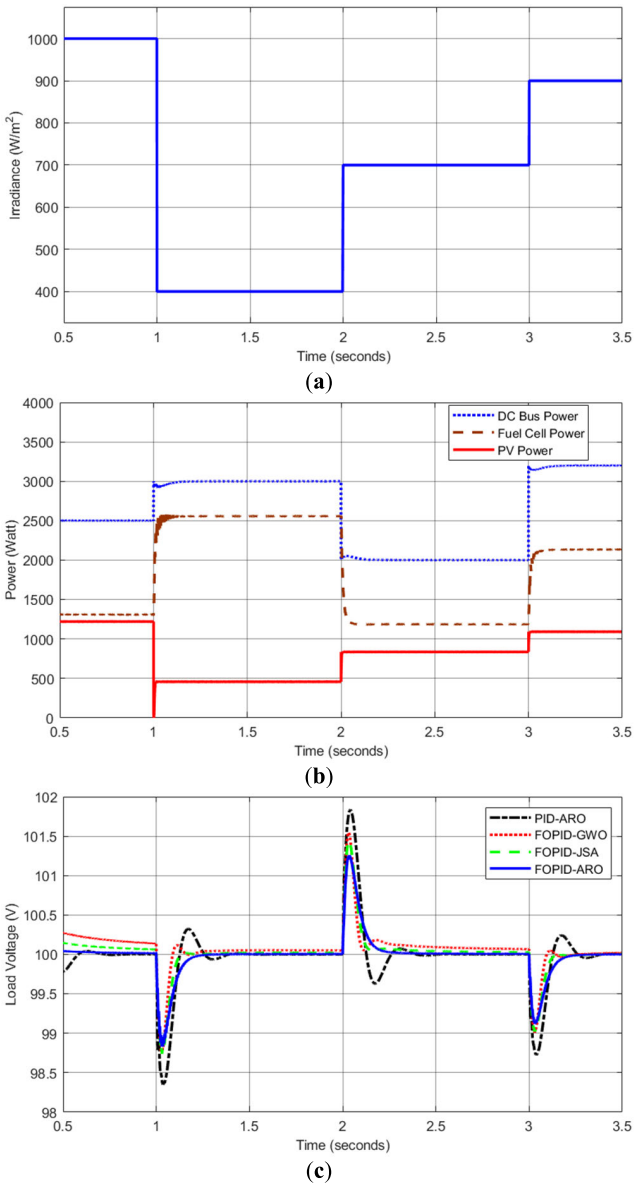

FIGURE 10. Case 3: (a) PV Irradiance; (b) Load, FC, and PV power; (c) Load voltage.

in Fig. 9a, the irradiance decreased from 1000 to 400 W/m^2, then increased from 400 to 700 W/m^2, and finally changed from 700 to 900 W/m^2 at times = 1, 2, 3 s respectively. Fig. 9b represents the impact of irradiance on PV, FC, and load powers, and Fig. 9c shows its effect on the load voltage. It is noted that FOPID-ARO has the least ISE, the least rise time, and better MPOS and MPUS, as shown in Table 7. The FOPID-ARO improved the MPOS by 30.96%, 25.98%, and 16.22% when compared to PID-ARO, FOPID-GWO, and FOPID-JSA respectively, and the MPUS by 32.43%, 3.54%, and 7% when compared to PID-ARO, FOPID-GWO, and FOPID-JSA, respectively. This means that the FOPID-ARO improved the dynamic response and decreased the error more than PID-ARO, FOPID-GWO, and FOPID-JSA.

TABLE 7. The transient parameters and ISE of load voltage for case 2.

Parameters	PID ARO	FOPID GWO	FOPID JSA	FOPID ARO
ISE	0.11907105	0.06976876	0.05561032	0.04993815
MPUS (%)	1.15323712	0.80790219	0.83794574	0.77927772
MPOS (%)	0.53016248	0.49445177	0.43688155	0.36601651
Rise time (s)	0.02348	0.02105	0.02129	0.02072

C. CASE (3): LOAD AND IRRADIANCE CHANGES

Sudden load and irradiance changes are applied to the system without considering temperature changes in PV. As seen in Fig. 10a, the irradiance decreases from 1000 to 400 W/m^2 at time = 1 s, increases from 400 to 700 W/m^2 at time = 2 s, and then increases once more from 700 to 900 W/m^2 at time = 3 s. Meanwhile, Fig. 10b illustrates the changes in the load.

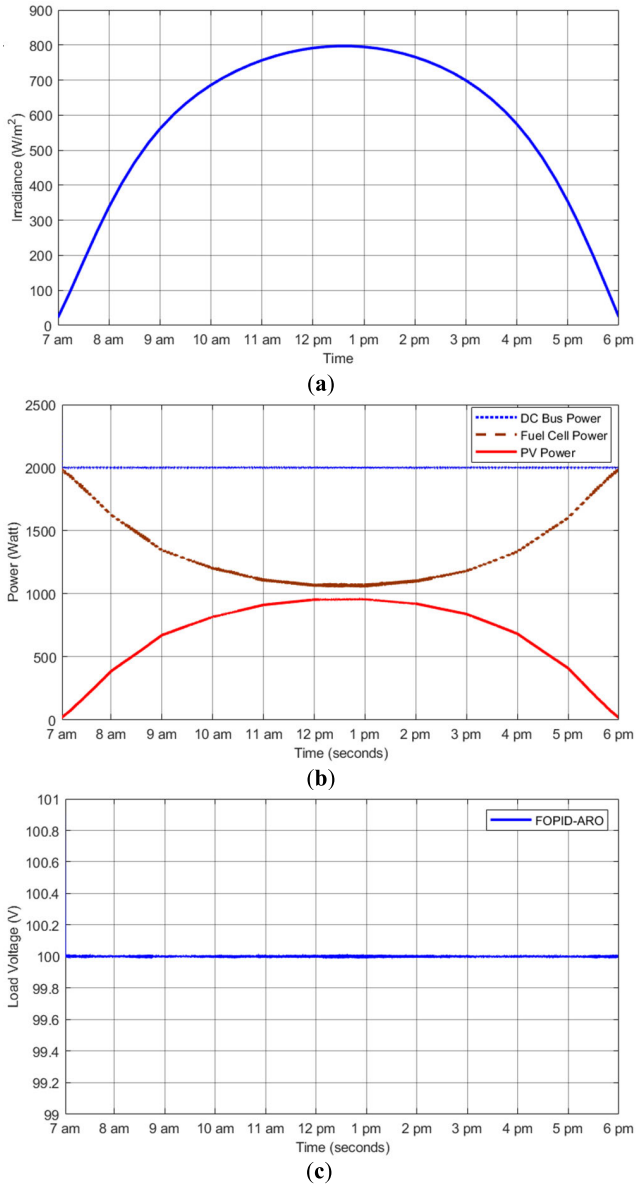

FIGURE 11. Case 4: (a) PV Irradiance; (b) Load, FC, and PV power; (c) Load voltage.

TABLE 8. The transient parameters and ISE of load voltage for case 3.

Parameters	PID ARO	FOPID GWO	FOPID JSA	FOPID ARO
ISE	0.523740921	0.249857675	0.242085609	0.222931912
MPUS (%)	1.649982395	1.257441585	1.262266863	1.171726823
MPOS (%)	1.836143765	1.548534962	1.443872192	1.255775656
Rise time	0.02409	0.02076	0.02118	0.0204

It increases from 2500 to 3000 W at time = 1 s, then decreases from 3000 to 2000 W at time = 2 s, and finally increases from 2000 to 3200 W at time = 3 s. Fig. 10c illustrates the impact of the sudden changes in load and irradiance on the load voltage. It is clear from Table 8 and Fig. 10c that FOPID-ARO has the least ISE, rise time, MPOS, and MPUS, which indicates that FOPID-ARO maintained the voltage closest to 100 V more than PID-ARO, FOPID-GWO, and FOPID-JSA.

D. CASE (4): REAL PV DATA

Here, actual data of irradiance of a day in February from Aswan (location south of Egypt) obtained from the Global Solar Atlas website [76] is used as the input of PV while maintaining a constant temperature of 25^0C for the PV and a constant load of 2000 W. The irradiance was recorded from 7 am to 6 pm and it changes between 20 W/m^2 to 797 W/m^2 as shown in Fig. 11a. Fig. 11b indicates the continuous change of PV and PEMFC power. The FOPID-ARO maintained the voltage constant, as shown in Fig. 11c. It was also noted that there were no overshoots, which means a good dynamic response.

VI. CONCLUSION

This paper introduces a FOPID controller with its parameters optimized by a new bio-inspired meta-heuristic algorithm (the ARO) to keep the PEMFC's voltage in a DC microgrid constant. In comparison to the PID controller, the FOPID controller exhibits greater flexibility and robustness since it has two more adjustable parameters, and the ARO algorithm has a small standard deviation and a fast convergence curve. The performance of FOPID-ARO is validated by comparing it to a PID controller tuned by ARO as well as a FOPID controller tuned by JSA and GWO algorithms under different conditions of load and irradiance variations in steps and real irradiance data. The ISE, MPOS, and MPUS are the parameters that are used to assess FOPID-ARO's performance. The FOPID-ARO shows the best response with an ISE of 0.204, 0.049, and 0.223 for case 1, case 2, and case 3 respectively and the least response time and shows an improvement in MPUS by 30.16%, 10.60%, and 9.46%, and in MPOS by 30.41%, 23.28%, and 14.85% when compared against PID-ARO, FOPID-GWO, and FOPID-JSA respectively for case 1, which indicates that the FOPID-ARO enhanced the dynamic response and the stability of the system more than the PID-ARO did and that it maintained the voltage closest to the required voltage (100 V). Moreover, the results also indicate the ARO algorithm yields better results than the JSA and the GWO algorithms.

In future research, wind energy sources, energy storage systems, and the continuous change of load will be considered in the microgrid, and real-world case studies will be conducted to show their applicability. Also, the control of the flow of hydrogen and oxygen in the fuel cell by FOPID to deliver the required power could be considered in the future.

ACKNOWLEDGMENT

This work was supported by the Researchers Supporting Project number (RSP2024R258), King Saud University, Riyadh, Saudi Arabia.

REFERENCES

[1] M. A. M. Shaheen, H. M. Hasanien, M. S. El Moursi, and A. A. El-Fergany, "Precise modeling of PEM fuel cell using improved chaotic MayFly optimization algorithm," *Int. J. Energy Res.*, vol. 45, no. 13, pp. 18754–18769, Oct. 2021, doi: 10.1002/er.6987.

[2] A. H. Yakout, H. M. Hasanien, and H. Kotb, "Proton exchange membrane fuel cell steady state modeling using marine predator algorithm optimizer," *Ain Shams Eng. J.*, vol. 12, no. 4, pp. 3765–3774, Dec. 2021, doi: 10.1016/j.asej.2021.04.014.
[3] A. Chammam, A. K. Tripathi, J. R. N. Alvarez, H. O. Alsaab, R. M. Romero-Parra, A. M. Mayet, and S. S. Abdullaev, "Multiobjective optimization and performance assessment of a PEM fuel cell-based energy system for multiple products," *Chemosphere*, vol. 337, Oct. 2023, Art. no. 139348, doi: 10.1016/j.chemosphere.2023.139348.
[4] C. Sun and H. Zhang, "Review of the development of first-generation redox flow batteries: Iron-chromium system," *ChemSusChem*, vol. 15, no. 1, Jan. 2022, Art. no. e202101798, doi: 10.1002/cssc.202101798.
[5] K. Gunawardane, N. Padmawansa, and H. Jayasinghe, "A review: Compatibility of fuel cells as promising technology for DC-microgrids," *Renew. Energy Environ. Sustainability*, vol. 9, p. 7, Jan. 2024, doi: 10.1051/rees/2024001.
[6] Z. Li, Z. Zheng, L. Xu, and X. Lu, "A review of the applications of fuel cells in microgrids: Opportunities and challenges," *BMC Energy*, vol. 1, no. 1, p. 8, Dec. 2019, doi: 10.1186/s42500-019-0008-3.
[7] A. Raza, M. K. Azeem, M. S. Nazir, and I. Ahmad, "Robust nonlinear control of regenerative fuel cell, supercapacitor, battery and wind based direct current microgrid," *J. Energy Storage*, vol. 64, Aug. 2023, Art. no. 107158, doi: 10.1016/j.est.2023.107158.
[8] O. Hafsi, O. Abdelkhalek, S. Mekhilef, M. A. Soumeur, M. A. Hartani, and A. Chakar, "Integration of hydrogen technology and energy management comparison for DC-microgrid including renewable energies and energy storage system," *Sustain. Energy Technol. Assessments*, vol. 52, Aug. 2022, Art. no. 102121, doi: 10.1016/j.seta.2022.102121.
[9] A. J. Riad, H. M. Hasanien, R. A. Turky, and A. H. Yakout, "Identifying the PEM fuel cell parameters using artificial rabbits optimization algorithm," *Sustainability*, vol. 15, no. 5, p. 4625, Mar. 2023, doi: 10.3390/su15054625.
[10] S. I. Selem, H. M. Hasanien, and A. A. El-Fergany, "Parameters extraction of PEMFC's model using manta rays foraging optimizer," *Int. J. Energy Res.*, vol. 44, no. 6, pp. 4629–4640, May 2020, doi: 10.1002/er.5244.
[11] B. Yang, J. Wang, L. Yu, H. Shu, T. Yu, X. Zhang, W. Yao, and L. Sun, "A critical survey on proton exchange membrane fuel cell parameter estimation using meta-heuristic algorithms," *J. Cleaner Prod.*, vol. 265, Aug. 2020, Art. no. 121660, doi: 10.1016/j.jclepro.2020.121660.
[12] Z. Shang, M. M. Hossain, R. Wycisk, and P. N. Pintauro, "Poly(phenylene sulfonic acid)-expanded polytetrafluoroethylene composite membrane for low relative humidity operation in hydrogen fuel cells," *J. Power Sources*, vol. 535, Jul. 2022, Art. no. 231375, doi: 10.1016/j.jpowsour.2022.231375.
[13] S. Ahmadi, S. Abdi, and M. Kakavand, "Maximum power point tracking of a proton exchange membrane fuel cell system using PSO-PID controller," *Int. J. Hydrogen Energy*, vol. 42, no. 32, pp. 20430–20443, Aug. 2017, doi: 10.1016/j.ijhydene.2017.06.208.
[14] M. Derbeli, M. Farhat, O. Barambones, and L. Sbita, "Control of PEM fuel cell power system using sliding mode and super-twisting algorithms," *Int. J. Hydrogen Energy*, vol. 42, no. 13, pp. 8833–8844, Mar. 2017, doi: 10.1016/j.ijhydene.2016.06.103.
[15] A. Souissi, "Adaptive sliding mode control of a PEM fuel cell system based on the super twisting algorithm," *Energy Rep.*, vol. 7, pp. 3390–3399, Nov. 2021, doi: 10.1016/j.egyr.2021.05.069.
[16] M. Derbeli, O. Barambones, and L. Sbita, "A robust maximum power point tracking control method for a PEM fuel cell power system," *Appl. Sci.*, vol. 8, no. 12, p. 2449, Dec. 2018, doi: 10.3390/app8122449.
[17] A. Sarvi, M. Parpaei, I. Soltani, and M. A. Taghikhani, "Eagle strategy based maximum power point tracker for fuel cell system," *IJE*, vol. 28, no. 4, pp. 529–536, Apr. 2015, doi: 10.5829/idosi.ije.2015.28.04a.06.
[18] A. Harrag and H. Bahri, "Novel neural network IC-based variable step size fuel cell MPPT controller," *Int. J. Hydrogen Energy*, vol. 42, no. 5, pp. 3549–3563, Feb. 2017, doi: 10.1016/j.ijhydene.2016.12.079.
[19] M. M. Gulzar, "Maximum power point tracking of a grid connected PV based fuel cell system using optimal control technique," *Sustainability*, vol. 15, no. 5, p. 3980, Feb. 2023, doi: 10.3390/su15053980.
[20] I. Nasiri Avanaki and M. Sarvi, "A new maximum power point tracking method for PEM fuel cells based on water cycle algorithm," *J. Renew. Energy Environ.*, vol. 3, no. 1, pp. 35–42, Feb. 2016, doi: 10.30501/jree.2016.70076.
[21] J. Liu, T. Zhao, and Y. Chen, "Maximum power point tracking with fractional order high pass filter for proton exchange membrane fuel cell," *IEEE/CAA J. Autom. Sinica*, vol. 4, no. 1, pp. 70–79, Jan. 2017, doi: 10.1109/JAS.2017.7510328.
[22] L. Fan and X. Ma, "Maximum power point tracking of PEMFC based on hybrid artificial bee colony algorithm with fuzzy control," *Sci. Rep.*, vol. 12, no. 1, p. 4316, Mar. 2022, doi: 10.1038/s41598-022-08327-5.
[23] K. P. S. Rana, V. Kumar, N. Sehgal, and S. George, "A NoveldPdIfeedback based control scheme using GWO tuned PID controller for efficient MPPT of PEM fuel cell," *ISA Trans.*, vol. 93, pp. 312–324, Oct. 2019, doi: 10.1016/j.isatra.2019.02.038.
[24] Z. Qi, J. Tang, J. Pei, and L. Shan, "Fractional controller design of a DC–DC converter for PEMFC," *IEEE Access*, vol. 8, pp. 120134–120144, 2020, doi: 10.1109/ACCESS.2020.3005439.
[25] Z. M. Ali, M. Al-Dhaifallah, S. F. Al-Gahtani, and T. Muranaka, "A new maximum power point tracking method for PEM fuel cell power system based on ANFIS with modified manta ray foraging algorithm," *Control Eng. Pract.*, vol. 134, May 2023, Art. no. 105481, doi: 10.1016/j.conengprac.2023.105481.
[26] H. Bahri and A. Harrag, "Ingenious golden section search MPPT algorithm for PEM fuel cell power system," *Neural Comput. Appl.*, vol. 33, no. 14, pp. 8275–8298, Jul. 2021, doi: 10.1007/s00521-020-05581-4.
[27] A. Fathy, H. Rezk, and T. M. Alanazi, "Recent approach of forensic-based investigation algorithm for optimizing fractional order PID-based MPPT with proton exchange membrane fuel cell," *IEEE Access*, vol. 9, pp. 18974–18992, 2021, doi: 10.1109/ACCESS.2021.3054552.
[28] H. Rezk, M. Aly, and A. Fathy, "A novel strategy based on recent equilibrium optimizer to enhance the performance of PEM fuel cell system through optimized fuzzy logic MPPT," *Energy*, vol. 234, Nov. 2021, Art. no. 121267, doi: 10.1016/j.energy.2021.121267.
[29] N. E. Benchouia, A. Derghal, B. Mahmah, B. Madi, L. Khochemane, and E. Hadjadj Aoul, "An adaptive fuzzy logic controller (AFLC) for PEMFC fuel cell," *Int. J. Hydrogen Energy*, vol. 40, no. 39, pp. 13806–13819, Oct. 2015, doi: 10.1016/j.ijhydene.2015.05.189.
[30] Y. Cao, Y. Li, G. Zhang, K. Jermsittiparsert, and M. Nasseri, "An efficient terminal voltage control for PEMFC based on an improved version of whale optimization algorithm," *Energy Rep.*, vol. 6, pp. 530–542, Nov. 2020, doi: 10.1016/j.egyr.2020.02.035.
[31] B. Salah, H. M. Hasanien, F. M. A. Ghali, Y. M. Alsayed, S. H. E. Abdel Aleem, and A. El-Shahat, "African vulture optimization-based optimal control strategy for voltage control of islanded DC microgrids," *Sustainability*, vol. 14, no. 19, p. 11800, Sep. 2022, doi: 10.3390/su141911800.
[32] A. Yasin, A. R. Yasin, M. B. Saqib, S. Zia, M. Riaz, R. Nazir, R. A. E. Abdalla, and S. Bajwa, "Fuel cell voltage regulation using dynamic integral sliding mode control," *Electronics*, vol. 11, no. 18, p. 2922, Sep. 2022, doi: 10.3390/electronics11182922.
[33] H. Hamedi, R. Khezri, S. Golshannavaz, and B. Ershadifard, "Efficient voltage control in proton exchange membrane fuel cell: An approach based on intelligent algorithms," *IETE J. Res.*, vol. 63, no. 2, pp. 216–224, Mar. 2017, doi: 10.1080/03772063.2016.1257375.
[34] H. A. Dhahad, K. E. Dagher, and A. S. Al-Araj, "Design of optimum SIMO-PID neural voltage-tracking controller for nonlinear fuel cell system based on a comparative study of various intelligent swarm optimization algorithms," *IOP Conf. Ser., Mater. Sci. Eng.*, vol. 1094, no. 1, Feb. 2021, Art. no. 012027, doi: 10.1088/1757-899X/1094/1/012027.
[35] S. Kart, F. Demir, I. Kocaarslan, and N. Genc, "Increasing PEM fuel cell performance via fuzzy-logic controlled cascaded DC–DC boost converter," *Int. J. Hydrogen Energy*, vol. 54, pp. 84–95, Feb. 2024, doi: 10.1016/j.ijhydene.2023.05.130.
[36] J. Li, T. Yu, and B. Yang, "Adaptive controller of PEMFC output voltage based on ambient intelligence large-scale deep reinforcement learning," *IEEE Access*, vol. 9, pp. 6063–6075, 2021, doi: 10.1109/ACCESS.2020.3049072.
[37] Z. Wang, G. Yi, and S. Zhang, "An improved fuzzy PID control method considering hydrogen fuel cell voltage-output characteristics for a hydrogen vehicle power system," *Energies*, vol. 14, no. 19, p. 6140, Sep. 2021, doi: 10.3390/en14196140.
[38] M. S. Borujeni and H. Zarabadipour, "Fuel cell voltage control using neural network based on model predictive control," in *Proc. Iranian Conf. Intell. Syst. (ICIS)*, Bam, Iran, Feb. 2014, pp. 1–5, doi: 10.1109/IRANIAN-CIS.2014.6802609.
[39] M. Karimi, J. Yahyazadeh, and A. Rezazade, "Controlling of proton exchange membrane fuel cell by model predictive controller based on ANFIS model," *Fuel Cells*, vol. 16, no. 5, pp. 530–537, Oct. 2016, doi: 10.1002/fuce.201600001.

[40] X. Li, Y. Qi, S. Li, P. Tunestal, and M. Andersson, "A multi-input and single-output voltage control for a polymer electrolyte fuel cell system using model predictive control method," *Int. J. Energy Res.*, vol. 45, no. 9, pp. 12854–12863, Jul. 2021, doi: 10.1002/er.6616.

[41] Q. Xu, N. Vafamand, L. Chen, T. Dragicevic, L. Xie, and F. Blaabjerg, "Review on advanced control technologies for bidirectional DC/DC converters in DC microgrids," *IEEE J. Emerg. Sel. Topics Power Electron.*, vol. 9, no. 2, pp. 1205–1221, Apr. 2021, doi: 10.1109/JESTPE.2020.2978064.

[42] M. Y. Silaa, M. Derbeli, O. Barambones, C. Napole, A. Cheknane, and J. M. G. De Durana, "An efficient and robust current control for polymer electrolyte membrane fuel cell power system," *Sustainability*, vol. 13, no. 4, p. 2360, Feb. 2021, doi: 10.3390/su13042360.

[43] S. A. G. K. Abadi, S. I. Habibi, T. Khalili, and A. Bidram, "A model predictive control strategy for performance improvement of hybrid energy storage systems in DC microgrids," *IEEE Access*, vol. 10, pp. 25400–25421, 2022, doi: 10.1109/ACCESS.2022.3155668.

[44] A. M. Agwa, T. I. Alanazi, H. Kraiem, E. Touti, A. Alanazi, and D. K. Alanazi, "MPPT of PEM fuel cell using PI-PD controller based on golden jackal optimization algorithm," *Biomimetics*, vol. 8, no. 5, p. 426, Sep. 2023, doi: 10.3390/biomimetics8050426.

[45] M. Elsisi, M.-Q. Tran, H. M. Hasanien, R. A. Turky, F. Albalawi, and S. S. M. Ghoneim, "Robust model predictive control paradigm for automatic voltage regulators against uncertainty based on optimization algorithms," *Mathematics*, vol. 9, no. 22, p. 2885, Nov. 2021, doi: 10.3390/math9222885.

[46] T. Hai, A. K. Alazzawi, J. Zhou, and H. Farajian, "Performance improvement of PEM fuel cell power system using fuzzy logic controller-based MPPT technique to extract the maximum power under various conditions," *Int. J. Hydrogen Energy*, vol. 48, no. 11, pp. 4430–4445, Feb. 2023, doi: 10.1016/j.ijhydene.2022.10.103.

[47] K. J. Reddy and N. Sudhakar, "ANFIS-MPPT control algorithm for a PEMFC system used in electric vehicle applications," *Int. J. Hydrogen Energy*, vol. 44, no. 29, pp. 15355–15369, Jun. 2019, doi: 10.1016/j.ijhydene.2019.04.054.

[48] F. A. S. Al-Taie and A. S. Al-Araj, "Development of predictive voltage controller design for PEM fuel cell system based on identifier model," *Int. J. Intell. Eng. Syst.*, vol. 16, no. 2, pp. 343–360, Feb. 2023, doi: 10.22266/ijies2023.0430.28.

[49] M. Derbeli, A. Charaabi, O. Barambones, and C. Napole, "High-performance tracking for proton exchange membrane fuel cell system PEMFC using model predictive control," *Mathematics*, vol. 9, no. 11, p. 1158, May 2021, doi: 10.3390/math9111158.

[50] R. Shalaby, M. El-Hossainy, B. Abo-Zalam, and T. A. Mahmoud, "Optimal fractional-order PID controller based on fractional-order actor-critic algorithm," *Neural Comput. Appl.*, vol. 35, no. 3, pp. 2347–2380, Jan. 2023, doi: 10.1007/s00521-022-07710-7.

[51] K. Bingi, R. Ibrahim, M. N. Karsiti, S. M. Hassan, and V. R. Harindran, "Real-time control of pressure plant using 2DOF fractional-order PID controller," *Arabian J. Sci. Eng.*, vol. 44, no. 3, pp. 2091–2102, Mar. 2019, doi: 10.1007/s13369-018-3317-9.

[52] S. Singh, V. K. Tayal, H. P. Singh, and V. K. Yadav, "Optimal design of fractional order PID controllers for solid oxide fuel cell system employing PSO algorithm," *AIUB J. Sci. Eng. (AJSE)*, vol. 21, no. 1, pp. 7–16, May 2022, doi: 10.53799/ajse.v21i1.225.

[53] D. Murugesan, K. Jagatheesan, P. Shah, and R. Sekhar, "Fractional order PIλDμ controller for microgrid power system using cohort intelligence optimization," *Results Control Optim.*, vol. 11, Jun. 2023, Art. no. 100218, doi: 10.1016/j.rico.2023.100218.

[54] H. Lotfi and A. Khodaei, "AC versus DC microgrid planning," *IEEE Trans. Smart Grid*, vol. 8, no. 1, pp. 296–304, Jan. 2017, doi: 10.1109/TSG.2015.2457910.

[55] T. L. Nguyen, J. M. Guerrero, and G. Griepentrog, "A self-sustained and flexible control strategy for islanded DC nanogrids without communication links," *IEEE J. Emerg. Sel. Topics Power Electron.*, vol. 8, no. 1, pp. 877–892, Mar. 2020, doi: 10.1109/JESTPE.2019.2894564.

[56] A. H. El-Ebiary, M. Mokhtar, M. A. Attia, and M. I. Marei, "A distributed adaptive control strategy for meshed DC microgrids," in *Proc. IEEE Conf. Power Electron. Renew. Energy (CPERE)*, Luxor, Egypt, Feb. 2023, pp. 1–6, doi: 10.1109/CPERE56564.2023.10119627.

[57] R. K. Sharma and S. Mishra, "Dynamic power management and control of a PV PEM fuel-cell-based standalone AC/DC microgrid using hybrid energy storage," *IEEE Trans. Ind. Appl.*, vol. 54, no. 1, pp. 526–538, Jan. 2018, doi: 10.1109/TIA.2017.2756032.

[58] M. B. Hossain, M. R. Islam, K. M. Muttaqi, D. Sutanto, and A. P. Agalgaonkar, "Modeling and performance analysis of renewable hydrogen energy hub connected to an AC/DC hybrid microgrid," *Int. J. Hydrogen Energy*, vol. 47, no. 66, pp. 28626–28644, Aug. 2022, doi: 10.1016/j.ijhydene.2022.06.172.

[59] S. Derakhshan, M. Shafiee-Rad, Q. Shafiee, M. R. Jahed-Motlagh, S. Sahoo, and F. Blaabjerg, "Decentralized voltage control of autonomous DC microgrids with robust performance approach," *IEEE J. Emerg. Sel. Topics Power Electron.*, vol. 9, no. 5, pp. 5508–5520, Oct. 2021, doi: 10.1109/JESTPE.2021.3054723.

[60] H. Khoramikia, S. M. Dehghan, and S. Hasanzadeh, "Droop control method based on fuzzy adaptive virtual resistance for DC microgrids," *Int. J. Power Electron.*, vol. 14, no. 2, pp. 197–215, 2021, doi: 10.1504/ijpelec.2021.117065.

[61] L. Wang, Q. Cao, Z. Zhang, S. Mirjalili, and W. Zhao, "Artificial rabbits optimization: A new bio-inspired meta-heuristic algorithm for solving engineering optimization problems," *Eng. Appl. Artif. Intell.*, vol. 114, Sep. 2022, Art. no. 105082, doi: 10.1016/j.engappai.2022.105082.

[62] V. M. Jyothi, T. V. Muni, and S. V. N. L. Lalitha, "An optimal energy management system for PV/battery standalone system," *Int. J. Electr. Comput. Eng. (IJECE)*, vol. 6, no. 6, p. 2538, Dec. 2016, doi: 10.11591/ijece.v6i6.pp2538-2544.

[63] D. Emara, M. Ezzat, A. Y. Abdelaziz, K. Mahmoud, M. Lehtonen, and M. M. F. Darwish, "Novel control strategy for enhancing microgrid operation connected to photovoltaic generation and energy storage systems," *Electronics*, vol. 10, no. 11, p. 1261, May 2021, doi: 10.3390/electronics10111261.

[64] M. H. Rashid, *Power Electronics Handbook: Devices, Circuits, and Applications*, 3rd ed. Burlington, MA, USA: Butterworth-Heinemann, 2011.

[65] M. H. Qais, H. M. Hasanien, S. Alghuwainem, K. H. Loo, M. A. Elgendy, and R. A. Turky, "Accurate three-diode model estimation of photovoltaic modules using a novel circle search algorithm," *Ain Shams Eng. J.*, vol. 13, no. 3, May 2022, Art. no. 101824, doi: 10.1016/j.asej.2022.101824.

[66] H. M. Hasanien, "Shuffled frog leaping algorithm for photovoltaic model identification," *IEEE Trans. Sustain. Energy*, vol. 6, no. 2, pp. 509–515, Apr. 2015, doi: 10.1109/TSTE.2015.2389858.

[67] M. Lokanadham and K. V. Bhaskar, "Incremental conductance based maximum power point tracking (MPPT) for photovoltaic system," *Int. J. Eng. Res. Appl.*, vol. 2, no. 2, pp. 1420–1424, 2012.

[68] A.-C. Braitor, G. C. Konstantopoulos, and V. Kadirkamanathan, "Current-limiting droop control design and stability analysis for paralleled boost converters in DC microgrids," *IEEE Trans. Control Syst. Technol.*, vol. 29, no. 1, pp. 385–394, Jan. 2021, doi: 10.1109/TCST.2019.2951092.

[69] O. Ibrahim, N. Z. Yahaya, N. Saad, and M. W. Umar, "MATLAB/simulink model of solar PV array with perturb and observe MPPT for maximising PV array efficiency," in *Proc. IEEE Conf. Energy Convers. (CENCON)*, Oct. 2015, pp. 254–258, doi: 10.1109/CENCON.2015.7409549.

[70] Y. Rao, Z. Shao, A. H. Ahangarnejad, E. Gholamalizadeh, and B. Sobhani, "Shark smell optimizer applied to identify the optimal parameters of the proton exchange membrane fuel cell model," *Energy Convers. Manag.*, vol. 182, pp. 1–8, Feb. 2019, doi: 10.1016/j.enconman.2018.12.057.

[71] J. Larminie and A. Dicks, *Fuel Cell Systems explained*, 2nd ed. Chichester, U.K.: Wiley, 2003.

[72] S. M. Njoya, O. Tremblay, and L.-A. Dessaint, "A generic fuel cell model for the simulation of fuel cell vehicles," in *Proc. IEEE Vehicle Power Propuls. Conf.*, Dearborn, MI, USA, Sep. 2009, pp. 1722–1729, doi: 10.1109/VPPC.2009.5289692.

[73] X. Lü, X. Miao, Y. Xue, L. Deng, M. Wang, D. Gu, and X. Li, "Dynamic modeling and fractional order PIλDμ control of PEM fuel cell," *Int. J. Electrochemical Sci.*, vol. 12, no. 8, pp. 7518–7536, Aug. 2017, doi: 10.20964/2017.08.12.

[74] S. Mirjalili, S. M. Mirjalili, and A. Lewis, "Grey wolf optimizer," *Adv. Eng. Softw.*, vol. 69, pp. 46–61, Mar. 2014, doi: 10.1016/j.advengsoft.2013.12.007.

[75] J.-S. Chou and D.-N. Truong, "A novel metaheuristic optimizer inspired by behavior of jellyfish in ocean," *Appl. Math. Comput.*, vol. 389, Jan. 2021, Art. no. 125535, doi: 10.1016/j.amc.2020.125535.

[76] (2023). *Global Solar Atlas*. Accessed: Dec. 10, 2023. [Online]. Available: https://globalsolaratlas.info/map?c=11.523088,8.173828,3

ANDREW J. RIAD was born in Cairo, Egypt, in January 1996. He received the B.Sc. degree in electrical engineering from the Faculty of Engineering, Ain Shams University, Cairo, in 2019. He is currently a Teaching Assistant with the Electrical Power and Machines Department, Faculty of Engineering, Ain Shams University. His research interests include renewable energy, power systems, optimization, and control.

HANY M. HASANIEN (Senior Member, IEEE) received the B.Sc., M.Sc., and Ph.D. degrees in electrical engineering from the Faculty of Engineering, Ain Shams University, Cairo, Egypt, in 1999, 2004, and 2007, respectively. From 2008 to 2011, he was a Joint Researcher with Kitami Institute of Technology, Kitami, Japan. From 2011 to 2015, he was an Associate Professor with the College of Engineering, King Saud University, Riyadh, Saudi Arabia. He is currently a Professor with the Electrical Power and Machines Department, Faculty of Engineering, Ain Shams University. He has authored, coauthored, and edited three books in the field of electric machines and renewable energy. He has published more than 320 papers in international journals and conferences. His research interests include modern control techniques, power systems dynamics and control, energy storage systems, renewable energy systems, and smart grids. He is an Editorial Board Member of *Electric Power Components and Systems*. His biography has been included in Marquis Who's Who in the World for its 28 edition, in 2011. He was awarded the Encouraging Egypt Award for Engineering Sciences in 2012, the Institutions Egypt Award for Invention and Innovation of Renewable Energy Systems Development in 2014, the Superiority Egypt Award for Engineering Sciences in 2019, and the Ain Shams University Appreciation Award in Engineering Sciences in 2022. He was the IEEE PES Egypt Chapter Chair (2020–2022). He is the Subject Editor of *IET Renewable Power Generation*, *Frontiers in Energy Research*, and *Electronics* (MDPI). He is also the Editor-in-Chief of *Ain Shams Engineering Journal* (Elsevier).

ZIA ULLAH (Member, IEEE) received the Ph.D. degree in electrical engineering from the Huazhong University of Science and Technology (HUST), Wuhan, China, in 2020. From 2020 to 2023, he was a Postdoctoral Research Fellow with the State Key Laboratory of Advanced Electromagnetic Engineering and Technology, School of Electrical and Electronic Engineering, HUST. He is currently an Associate Professor with the School of Electrical Power, Civil Engineering and Architecture, Shanxi University, Taiyuan, China. His research interests include power system optimization, intelligent power distribution systems, distribution system planning with RES, power system operation and control, EV integrated distribution networks optimization, EV charging station designing, and EV scheduling optimization.

ABDULAZIZ ALKUHAYLI (Member, IEEE) received the B.Sc. degree in electrical engineering from King Saud University, Riyadh, Saudi Arabia, in 2006, the M.S. degree in electrical engineering from Missouri University of Science and Technology, Rolla, MO, USA, in 2013, and the Ph.D. degree in electrical engineering from North Carolina State University, Raleigh, NC, USA, in 2018. From 2006 to 2009, he was an Operation Engineer with the Energy Control Center, Saudi Electricity Company. He is currently an Assistant Professor with the Department of Electrical Engineering, King Saud University. His research interests include energy management, renewable energy systems, flexible AC transmission systems, power system stability, and smart grids. He received the IEEE Electromagnetic Compatibility Society Best Symposium Paper Award in 2011.

AHMED H. YAKOUT received the bachelor's and master's degrees from the Electrical Power and Machines Department, Faculty of Engineering, Ain Shams University, Cairo, Egypt, in 2000 and 2005, respectively, and the Ph.D. degree in electrical engineering from the University of Strathclyde, Glasgow, U.K., in 2010. He is currently an Associate Professor with the Faculty of Engineering, Ain Shams University. His research interests include electrical power systems analysis, stability, control, renewable energy, artificial intelligence, optimization, smart grids, fuzzy, and adaptive control.